Amphipathic Janus nanofibers aerogel for efficient solar steam generation

Rui Wang[1], Jinshuo Deng[1], Ping Wu[1], Qianli Ma[1], Xiangting Dong[1], Wensheng Yu[1], Guixia Liu[1], [2], and Lei Liu[1]

[1]Changchun University of Science and Technology
[2]Changchun university of science and technology

June 5, 2023

Abstract

Solar steam generation is a promising water purification technology due to its low-cost and environmentally friendly applications in water purification and desalination. However, hydrophilic or hydrophobic materials alone are insufficient in achieving necessary characteristics for constructing high-quality solar steam generators with good comprehensive properties. Herein, novel hydrophile/hydrophobe amphipathic Janus nanofibers aerogel is designed and used as a host material for preparing solar steam generators. The product consists of an internal cubic aerogel and an external layer of photothermal materials. The internal aerogel is composed of electrospun amphipathic Janus nanofibers. Owing to the unique composition and structure, the prepared solar steam generator integrates the features of high water evaporation rate (2.944 kg·m-2·h-1 under 1 kW m-2 irradiation), self-floating, salt-resisting, and fast performance recovery after flipping. Moreover, the product also exhibits excellent properties on desalination and removal of organic pollutants. Compared with traditional hydrophilic aerogel host material, the amphipathic Janus nanofibers aerogel brings much higher water evaporation rate and salt resistance.

Response to the Comments

Dear Editor,

Thank you very much for your hard work in processing our manuscript and also thanks a lot for the valuable comments and suggestions to improve our paper. Based on these comments, we have made careful corrections on the manuscript, and the corresponding revisions in the body text of the manuscript are highlighted in yellow background. We submit a revised manuscript here. The following are our point-to-point response to reviewers concerning the comments about the manuscript.

Reviewer #1:

The manuscript ”Amphipathic Janus nanofibers aerogel for efficient solar steam generation.” by Rui Wang et al. presents a novel hydrophile/hydrophobe amphipathic Janus nanofibers aerogel, which can be used as a host material for constructing the solar steam generator. The prepared solar steam generator exhibits excellent water evaporation, desalination and removal of organic pollutants performances. I have several concerns as follows:

Comment 1: Currently, there are many solar evaporators with Janus structure. What are the advantages of amphipathic Janus nanofibers aerogel evaporator compared to other Janus evaporators?

Response 1: As the respected reviewer mentioned, many solar evaporators with Janus structure have been reported. However, all of these reported solar evaporators are “macroscopically” Janus structure. As we described in the original manuscript: “To date, there have been many reports on macroscopical combination of hydrophilic and hydrophobic materials for SSG, that is, hydrophilic and hydrophobic materials are separated in different regions of the reported solar steam generators, but no research on their microscopical combination can be found", the already reported solar evaporators with Janus structure can fall into macroscopical combination of hydrophilic and hydrophobic materials, in which the hydrophobic materials only provide the function of floating. In our work, the amphipathic Janus nanofibers aerogel is "microscopically" Janus structure. In addition to providing self-floating function, the hydrophobic PVB components also can limit internal water content, suppress salt deposition and inhibit volume expansion of swollen CA components (the discussion on inhibition of volume expansion is newly added in the revised manuscript), and these properties are owing to the "microscopically" Janus structure of amphipathic Janus nanofibers aerogel. In order to more clearly point out the advantages of this "microscopically" Janus structure, relevant parts of the manuscript are revised.

Comment 2: The authors may need to evaluate the performance of the material after 10 cycles to further show that the long-term evaporation does not affect the material performance.

Response 2: As the respected reviewer suggested, the reusability testing is extended to 20 cycles, as shown in the revised manuscript. Due to the one-month time limit for submitting the revised manuscript, we can only conduct 20 cycles testing at present, and longer reusability testing can be provided when the final manuscript is submitted.

Comment 3: The real photographs of CA//PVB Janus nanofibers aerogel and the solar steam generator should be provided.

Response 3: As the respected reviewer's request, the photographs of CA//PVB Janus nanofibers aerogel and the solar steam generator are provided in the revised manuscript.

Comment 4: In this paper, the effects of aerogel density, loading capacity and photothermal material composition on its performance were studied respectively, and detailed conclusions and comprehensive results should be given.

Response 4: The detailed conclusions and comprehensive results for the optimized parameters are clarified in the revised manuscript.

Reviewer #2:

In this manuscript, the authors described a hydrophile/hydrophobe amphipathic Janus nanofibers aerogel for constructing the solar steam generator. The water evaporation rate can reach 2.944 kg m^{-2} h^{-1} with an energy efficiency of 91.05% under 1 sun. The flipping issue is also involved, resulting in a quick recovery of the water evaporation rate. Overall, this article is well-organized but the novelty and some crucial point of this work needs further refinement. Thus, I do not think that this work qualified enough to be published on Advanced Functional Material:

Comment 1: The authors mentioned that: "hydrophobic or hydrophilic material alone hardly achieves adequate property for constructing solar steam generators." However, many works using hydrophilic materials exhibit completive, even higher evaporation rates compared to that proposed in this manuscript (2.944 $kg{\cdot}m^{-2}{\cdot}h^{-1}$ under 1 kW m^{-2} irradiation).

Response 1: We acknowledge the respected reviewer's observation that hydrophilic materials can provide high water evaporation rates. Nevertheless, the solar steam generators consisting only of hydrophilic materials hardly independently float on water surface, and additional supporting materials are necessary. Besides, hydrophilic materials are not effective in preventing the shuttle of salt ions. As for the sentence mentioned by the respected reviewer, what we wanted to express is "hydrophilic or hydrophobic materials alone are insufficient in achieving necessary characteristics for constructing high-quality solar steam generators with good comprehensive properties", high water evaporation rate is just one of important characteristics for solar steam generators, and the properties such as self-floating, salt resistance, and stability are also crucial factors. In order to avoid misunderstanding, we have modified the relevant statement.

Comment 2: According to the SEM images (Figure 1) of nanofibers aerogel and solar steam generator, the surface and the pores of aerogel are filled by photothermal materials. The hydrophilicity/hydrophobicity of nanofiber still plays a key role in water evaporation. The floating feature is due to the hydrophobic/hydrophilic Janus nanofiber or just because of the density change? Will the blended single nanofiber show a similar property? Blended electrospinning instead of parallel spinning is suggested to fabricate non-Janus structural nanofiber for comparison. The merits of hydrophile/hydrophobe amphipathic Janus nanofiber structure should be highlighted and completely clarified since it is the prominent description in the Title.

Response 2: Thanks a lot for the respected reviewer's good suggestions! Accordingly, CA-PVB blended nanofibers aerogel is fabricated by single-nozzle electrospinning for comparison. It is found that the solar steam generator based on CA-PVB blended nanofibers aerogel shows a very poor water evaporation rate, and relevant discussion is provided in the revised manuscript. Besides, the cycling performance of the solar steam generator based on CA nanofibers aerogel is added in the revised manuscript. The merits of the amphipathic Janus nanofibers aerogel can be highlighted and completely clarified based on these supplemental experimental results.

Comment 3: All figures should be mentioned in the text in numerical or alphabetical order. Namely, Figure 1a should be organized and mentioned before Figure 1b-e.

Response 3: Figure 1 has been modified as requested.

Comment 4: The authors investigated the influence of water states (BW, IW and FW) on evaporation rate due to the silica NPs in detail. But the nanofibers aerogel evaporator is a 3D evaporator, the environmental enhancement on evaporation should be considered as well.

Response 4: There are indeed many other reports on 3D evaporators that have investigated environmental enhancement effects such as airflow, irradiation angle, and cold evaporation. However, these environmental enhancement effects are significant only when the evaporators are exposed above the water surface at considerable heights. That is, the exposed side area is large enough. Although our products are also 3D evaporators, their height above the water surface is less than 1 cm and can be considered negligible in terms of environmental enhancement. In addition, because there is no unified standard of experimental parameters for environmental enhancement in this field, it is hard to select widely approved experimental conditions. Based on the above reasons, the ambient temperature, humidity and irradiation angle are constant in this work, and no airflow is engaged. Thanks a lot for your understanding in advance!

Comment 5: The authors claimed that "the flipping recovery of the solar steam generator is an important issue in practical outdoor applications." and flipping experiments of a cubic solar steam generator were carefully conducted. On the other hand, purified water collection is still a key process for solar desalination from the practical view, which the authors also present in the manuscript. So, is the flipping recovery experiments carried out in the evaporation/collection system more meaningful rather than the cubic evaporator?

Response 5: Due to the lack of a standardized preparation protocol for water collection systems in this field, the performance of solar steam generators in different collection systems is influenced by factors such as material, shape, and size of collection systems. To eliminate these factors on experimental results, it is common practice in this industry to evaluate the performance of solar steam generators outside of the collection system whenever possible, and only desalination and contaminant removal properties are tested within the collection system. We conducted experimental design in accordance with the methodology employed in relevant literature.

Comment 6: What's the purified water collection rate in the acrylic tank?

Response 6: The purified water collection rate in the used acrylic tank is provided in the revised manuscript. Please note that the water collection rate is influenced not only by the performance of the solar steam generator itself, but also by the material, shape and size of the collection system. Therefore, this value should be used as a reference only.

We have tried our best to modify the manuscript in order to meet the requirements of reviewers, and we sincerely look forward to receiving your positive responses!

Thanks a lot for the time and efforts you have spent on our paper!

Sincerely yours,

Prof. Qianli Ma (Corresponding author)

Article category: Full Paper

Subcategory: Solar steam generation

Amphipathic Janus nanofibers aerogel for efficient solar steam generation

Rui Wang, Jinshuo Deng, Ping Wu, Qianli Ma*, Xiangting Dong*, Wensheng Yu, Guixia Liu, Jinxian Wang, and Lei Liu

Rui Wang, Jinshuo Deng, Ping Wu, Qianli Ma*

Chongqing Research Institute, Changchun University of Science and Technology, Chongqing 401135, China
E-mail: maqianli@cust.edu.cn

Xiangting Dong*, Wensheng Yu, Guixia Liu, Jinxian Wang, Lei Liu Key Laboratory of Applied Chemistry and Nanotechnology at Universities of Jilin Province, Changchun University of Science and Technology, Changchun 130022, China

E-mail: xtdong@cust.edu.cn

Keywords: solar steam generation, photothermal materials, electrospinning, aerogels, solar desalination

Abstract: Solar steam generation is a promising water purification technology due to its low-cost and environmentally friendly applications in water purification and desalination. However, hydrophilic or hydrophobic materials alone are insufficient in achieving necessary characteristics for constructing high-quality solar steam generators with good comprehensive properties. Herein, novel hydrophile/hydrophobe amphipathic Janus nanofibers aerogel is designed and used as a host material for preparing solar steam generators. The product consists of an internal cubic aerogel and an external layer of photothermal materials. The internal aerogel is composed of electrospun amphipathic Janus nanofibers. Owing to the unique composition and structure, the prepared solar steam generator integrates the features of high water evaporation rate (2.944 $kg{\cdot}m^{-2}{\cdot}h^{-1}$under 1 kW m^{-2} irradiation), self-floating, salt-resisting, and fast performance recovery after flipping. Moreover, the product also exhibits excellent properties on desalination and removal of organic pollutants. Compared with traditional hydrophilic aerogel host material, the amphipathic Janus nanofibers aerogel brings much higher water evaporation rate and salt resistance.

1. Introduction

Solar steam generation (SSG) is an emerging water purification technology and has become a research hotspot in the field of water treatment in recent years.[1-3] Its working principle is to utilize solar energy to convert water from waste water or sea water into water steam which is then collected and condensed into fresh water. This technique can separate water from contaminants and other impurities in a process similar to the water cycle in the natural environment. Hence, it is an eco-friendly and low-cost water purification strategy that does not require extra energy.

However, due to the low light absorption and photothermal conversion efficiency of water, an efficient SSG process requires placing the materials with the function of photothermal conversion on the surface of water to realize interfacial heating, and these materials are usually called solar steam generators or solar absorbers.[4-6] To date, many types of solar steam generators, such as photothermal aerogels[7], hydrogels[8], foams[9], membranes[10], have been fabricated. Macroscopically, solar steam generators can be classified into one-dimensional (1D), 2D and 3D materials. Among them, 3D solar steam generators are considered to be the most promising materials owing to their high water evaporation rates and versatility.[11-13] In general, 3D solar steam generators have large thicknesses, which is conductive to reduce thermal dissipation from evaporation surface to bulk water and also enhance the energy efficiency by allowing multiple reflections of light inside the 3D solar steam generators. Moreover, the 3D structure provides more feasibility for structural design. By far, many different shapes of 3D solar steam generators have been prepared to endow the materials with the features such as self-floating[14], salt-resisting[15], self-cleaning[16], and cold evaporation[17].

The solar steam generators based on 3D aerogels are hot spot of current researches.[18-20] As a commonly used method for preparing 3D aerogels, electrospinning combined with freeze drying has been developed for several years.[21-24] In addition to their applications in SSG, electrospun 3D aerogels also exhibit other application prospects in thermal insulation[25], tissue engineering[26], photocatalysis[27], oil/water separation[28] and *etc* . However in the existing reports, without taking into account the post-processing procedures, the aerogels prepared by direct electrospinning are either completely hydrophilic or hydrophobic, which causes some issues in the application of SSG. Although hydrophilic aerogels can pump water to the evaporation surface, the excessive water inside the aerogels acts as a "thermal bridge" which results in serious thermal dissipation from evaporation surface to bulk water. For another, because hydrophilic aerogels cannot float on the water surface, additional supporting materials are usually necessary. By contrast, completely hydrophobic aerogels are hardly suitable for preparing solar steam generators due to the incapability of pumping water to the evaporation surface. Therefore, it is rational that proper combination of hydrophilic and hydrophobic materials should be an ideal solution for constructing solar steam generators. To date, there have been many reports on macroscopical combination of hydrophilic and hydrophobic materials for SSG[29-32], that is, hydrophilic and hydrophobic materials are separated in different regions of the reported solar steam generators, and some reported solar steam generators possess Janus structure[32-37]. The term "Janus structure" in these works refers to bilayer structure at the macro level, where the hydrophilic materials acts as a water pump, while the hydrophobic materials enable the solar steam generators to float on water surface. However, no research on microscopical combination of hydrophilic and hydrophobic materials can be found. Therefore, it is meaningful to construct a solar steam generator composed of microscopically bonded hydrophilic and hydrophobic materials and discover the advantages of this design philosophy.

Herein, novel hydrophile/hydrophobe amphipathic Janus nanofibers aerogel is first proposed and used as a host material for constructing the solar steam generator. Every amphipathic Janus nanofiber in the aerogel is composed of a hydrophilic cellulose acetate (CA) side and a hydrophobic polyvinyl butyral (PVB) side, forming a "microscopically" Janus structure, as depicted in **Figure 1** a. Such peculiar architecture and composition endow the aerogel with water-pumping, self-floating, heat-insulating, salt-resisting properties and excellent continuous working stability which are crucial characteristics for solar steam generators. To obtain the solar steam generator, the amphipathic Janus nanofibers aerogel is coated by photothermal materials consisted of carbon nanotubes (CNTs), silicon dioxide nanoparticles (SiO_2 NPs) and polydopamine (PDA), in which CNTs play a prominent role in photothermal conversion, SiO_2 NPs can regulate the water state, and PDA is the adhesive and contributes to photothermal conversion as well. The prepared solar steam generator exhibits excellent water evaporation, desalination and removal of organic pollutants performances. Another advantage of the solar steam generator is that its water evaporation performance can quickly recover after it is flipped on the water surface, which is a meaningful feature for dealing with dynamic water environment.

2. Results and Discussion

2.1. Structural Characterization

The microstructures of CA nanofibers, PVB nanofibers, CA//PVB Janus nanofibers, CA//PVB Janus nanofibers aerogel and the surface of the solar steam generator are determined by SEM observation. As shown in Figure 1b and c, the prepared CA nanofibers and PVB nanofibers have similar morphologies, and their diameters are about 600 nm. Figure 1d reveals that every CA//PVB Janus nanofiber is composed of two tightly adjacent nanofibers whose diameters are both about 600 nm, indicating a typical Janus nanofiber structure. Although it is hard to determine the difference in the chemical compositions of the two adjacent nanofibers by existing material characterization techniques because CA and PVB both consist of elemental C, H and O, it is still safe to conclude that the two adjacent nanofibers are respectively comprised of CA and PVB according to the existing reports on fabrications of Janus nanofibers *via* parallel electrospinning. In these reports, it has been proved that the two adjacent nanofibers of a Janus nanofiber are respectively derived from two spinning solutions for parallel electrospinning.[38-40] Figure 1e manifests that the Janus nanofibers in the aerogel are successfully crosslinked, which reinforces the shape stability of the aerogel. The crosslinked Janus nanofibers have slightly larger sizes than those before crosslinking, which can be due to the swelling of polymer nanofibers in the solution containing crosslinking agent and volume expansion during thermal crosslinking. Furthermore, it can be noticed that micron-sized irregular channels exist among the Janus nanofibers and can allow water transfer. Figure 1f-h are SEM imagery of the surface of solar steam generator at different levels of magnification. The CNTs, with the diameters of *ca.* 40 nm, are evenly distributed on the product surface, and SiO_2 NPs are attached to the CNTs. Hierarchical pores are formed among the CNTs and SiO_2 NPs, which can facilitate water transfer and steam escape.

2.2. Hydrophilicity

The hydrophilicities of CA nanofibers, PVB nanofibers, CA//PVB Janus nanofibers and photothermal materials are measured, as presented in **Figure S3** . CA nanofibers can completely absorb the water droplet within 0.5 s, manifesting their very high hydrophilicity. On the contrary, the water droplet shows a stable contact angle of about 130 ° on hydrophobic PVB nanofibers, which indicates that PVB nanofibers alone are not a suitable host material for constructing solar steam generators because water cannot permeate through PVB nanofibers. As for the CA//PVB Janus nanofibers, the water droplet is slowly absorbed, which brings an important benefit: the water supply rate is not too high in SSG process. Previous studies have found that too fast water supply, normally caused by too high hydrophilicity of host materials, results in decreased temperature of evaporation surface and reduced water evaporation rate.[41] Additionally, the hydrophile/hydrophobe amphipathic CA//PVB Janus nanofibers can float on water surface, whereas CA nanofibers cannot. Therefore, from the perspective of hydrophilicity, CA//PVB Janus nanofibers should be more applicable for constructing solar steam generators compared with CA nanofibers and PVB nanofibers. As seen from Figure S3d, the water droplet is quickly absorbed into photothermal materials, which is because the used CNTs, SiO_2 NPs and PDA are hydrophilic. Hence, in the prepared solar steam generator, the water pumped through the CA//PVB Janus nanofibers aerogel can quickly and uniformly spread all over the outer photothermal materials layer owing to the high hydrophilicity of the photothermal materials, which is conducive to water evaporation.

2.3. Solar Steam Generation Performance

Firstly, the performance of solar steam generation using pure water as analyte is evaluated to optimize the product composition. The impacts of aerogel density, loading amount and composition of the photothermal materials are respectively studied.

The density of an aerogel mainly affects saturation water content of the solar steam generator. As seen from **Figure 2** a, the density of solar steam generator becomes larger with increased mass ratio of Janus nanofibers to dispersion medium in freeze drying process, while the saturation water content is decreased. Figure 2b shows the water evaporation performances of the solar steam generators. As the density increases, the solar steam generators display increased first and then decreased water evaporation rates. The increase in water evaporation rates can be attributed to alleviative thermal dissipation from evaporation surface to bulk water caused by decreased water contents in the solar steam generators. The thermal conductivities of CA and PVB are determined to be 0.17 W $m^{-2}K^{-2}$ and 0.23 W $m^{-2}K^{-2}$, respectively, which are substantially lower than that of water (0.59 W m^{-2} K^{-2}). Hence, decreased water content in the solar steam generator is beneficial to reduce heat dissipation and increase the temperature of evaporation surface. As seen in Figure 2c, the temperature (after one-hour irradiation) of evaporation surface increases with increased density of the solar steam generator, whereas that of the bulk water is reduced. However, the increased density of solar steam generator simultaneously results in increased resistance of water transfer, which is negative to water evaporation. Therefore, appropriate aerogel density is an important basis to ensure high-efficient water evaporation.

Secondly, optimized loading amount of photothermal materials is explored, as shown in Figure 2d. It can be seen that the solar steam generator with the photothermal materials of 0.016 g·cm^{-2} exhibits the best performance. Insufficient photothermal materials cannot produce enough heat to sustain rapid water evaporation. On the contrary, because the pores in the photothermal materials are small (at the nanoscale), excessive photothermal materials leads to too high resistance of water transfer and thus decreases water evaporation rate.

Thirdly, the dosages of raw materials for preparing photothermal materials are optimized. To start with, the concentration of dopamine is fixed (y=2.4), while the dosage of TEOS is varied (x=0.1, 0.2, 0.3, 0.4, 0.5), and relevant SSG results are shown in Figure 2e. With the increased dosage of TEOS (i.e. enlarged content of SiO_2NPs), the water evaporation rates reveal an increasing trend at the beginning and then decrease when x>0.3. To explain this phenomenon, at first, the surface temperatures of the solar steam generators are measured. As seen from Figure 2f, with the gradual increase of SiO_2NPs content, the surface temperatures of the solar steam generators show a falling trend, which can be ascribed to the fact that the SiO_2 NPs, although have been modified with dark-colored PDA, possess relatively lower photothermal conversion performance than CNTs. The light absorption spectra of the solar steam generators shown in Figure 2g can prove the degradation of light absorption performance with increased SiO_2 NPs content. Therefore, from the perspective of surface temperature, the performance enhancement of the products within x=0.1 to 0.3 cannot be well explained. It has been known that there are three kinds of water in a material: bound water (BW), intermediate water (IW) and free water (FW).[42] Among them, BW is the water molecule in direct contact with the hydrophilic materials. Because strong chemical bonds are formed between BW and the materials, BW is difficult to evaporate. The FW is relatively far from the adsorption materials, and its property is consistent with the bulk water. The IW is sandwiched between the BW and FW. Due to the interaction between the adjacent BW and adsorption materials, the hydrogen bonds between IW and BW are weakened, leading to the lowest energy required for the evaporation of IW. That is, IW has the lowest evaporation enthalpy among the three kinds of water.[43] In this study, SiO_2 NPs can fill in the gaps among CNTs and thus regulate the water state in the photothermal materials. Figure 2h visually depicts the increased proportion of IW and reduced proportion of FW when more SiO_2 NPs are introduced. In addition, the variation of BW can be ignored because BW is in monomolecular type and its proportion is very low among the three kinds of water. It has been reported that the ratio of IW to FW in a material can be quantitatively measured by Raman spectroscopy, and Gaussian function can be used to fit the peaks at 3233 cm^{-1}, 3401 cm^{-1}, 3514 cm^{-1} and 3630 cm^{-1}.[44] The peaks at 3233 cm^{-1} and 3401 cm^{-1} correspond to the in-phase and out-of-phase vibration modes of O-H bonds in water that forms four hydrogen bonds with surrounding water molecules, which represent the existence of FW. The peaks at 3514 cm^{-1}and 3630 cm^{-1} are assigned to the symmetric and asymmetric stretching of O-H bonds in the weakened hydrogen bonds, which are the characteristic peaks of IW that is relatively weakly affected by hydrogen bond. The ratio of the fitted peak areas of the two kinds of water is the molar ratio of the two kinds of water. The Raman spectra of the hydrated photothermal materials are given in **Figure S4** . According to the calculation of fitted peak areas, the molar ratios of IW to BW in these samples (x=0.1, 0.2, 0.3, 0.4, 0.5) are 0.38, 0.52, 0.67, 0.71, 0.73, respectively, which further demonstrates increased proportion of IW when more SiO_2 NPs are introduced. However, excessive SiO_2 NPs (x=0.4 and 0.5) cannot substantially increase the proportion of IW, but make the light absorption performance of the photothermal materials continuously degrade, as revealed in Figure 2g, resulting in the decreased water evaporation rate.

The impact of PDA is evaluated while the ratio of CNTs and SiO_2 NPs is fixed (x=0.3). Here, the PDA mainly acts as an adhesive in the photothermal materials, and also contributes to photothermal conversion due to its dark color. In order to study the adhesive performance of the PDA, the solar steam generators with different PDA contents were completely immersed in water for 1 h and then naturally dried. The mass changes of the samples before and after soaking are given in Figure 2i. When PDA is not enough (y=0.8 and 1.6), some photothermal materials fall off the solar steam generators and disperse into the water, and obvious mass losses of the samples are found. When sufficient PDA is introduced (y[?]2.4), the photothermal materials can be stable on the solar steam generators. In spite of this, excess PDA content is still detrimental because the light absorption performance is impaired and the water evaporation rate is decreased, as indicated in Figure 2i-l.

Based on the above, the optimized parameters for preparing the solar steam generator are as follows: the mass ratio of nanofibers to water is 0.0500:1 in the dispersion medium for freeze drying; the dosages of TEOS (x) and dopamine (y) are respectively 0.3 and 2.4 for preparing the photothermal materials; the loading amounts of the photothermal materials is 0.016 g*cm^{-2}. The optimized solar steam generator can provide a state-of-the-art water evaporation rate (2.944 kg m^{-2} h^{-1}) under 1 sun irradiation. Next, the impact of light irradiation intensity on water evaporation rate and energy efficiency is investigated. Light irradiation intensity is one of the important factors affecting the water evaporation rate. In order to further explore the water evaporation performance of the optimized solar steam generator under different light irradiation intensities, 0.5, 1, 1.5 and 2 suns are respectively adopted. As shown in **Figure 3** a and b, water evaporation rates of 1.486 kg*m^{-2}*h^{-1}, 2.944 kg*m^{-2}*h^{-1}, 4.469 kg*m^{-2}*h^{-1} and 5.899 kg*m^{-2}*h^{-1} are achieved when the irradiation intensities are 0.5, 1, 1.5 and 2 suns, while the energy efficiencies are 88.74 %, 91.05 %, 91.94 % and 92.83 %, respectively. In most reports on solar steam generators, energy efficiency generally increases with the increase of irradiation intensity.[10,32,45] Of the solar steam generator prepared in this work, the evaporation surface temperature significantly rises with increased irradiation intensity, whereas the temperature of bulk water varies little, which indicates excellent thermal insulation performance of the prepared solar steam generator. The experimental results show that the product possesses superior SSG performance under different irradiation intensities, suggesting its application potential in the natural environment where sunlight intensity changes frequently and the conditions with concentrated sunlight by using optical concentrators such as convex lens and heliostats.

The stability of solar steam generators is also a key factor affecting their practical application. Hence, the real-time water content, continuous working stability and reusability of the prepared solar steam generator are studied. The test method of real-time water content is as following: the solar steam generator is taken out from bulk water every 20 min during SSG process, the water drops on the surface of solar steam generator are wiped off by using filter papers, and then the weight of the waterlogged solar steam generator is measured and compared with that of the dry solar steam generator. Continuous working stability is evaluated by ten-hour uninterrupted irradiation, and the mass changes of water are recorded per hour to calculate hourly water evaporation rates. The reusability is studied by twenty-cycle SSG processes. Continuous ten-hour irradiation is employed for each cycle, and the solar steam generator is dried after each cycle.

The test results are shown in **Figure 4** a-c. The water content of the solar steam generator is basically constant in SSG process, indicating continuous and stable water pumping. The water evaporation rates remain steady within both ten-hour continuous SSG process and twenty -cycle reusing. These results manifest that the product possesses excellent stability and has great application potential.

An unavoidable problem with solar steam generators in practical outdoor applications is the flip of the generators due to the effects of wind, water wave and *etc* . In order to accommodate this situation, the prepared cubic solar steam generator is fully covered with photothermal materials on its six surfaces, so that its all surfaces can be used for water evaporation, as depicted in Figure 4d. The performance recovery of the solar steam generator after flipping is investigated, and the specific experimental methods are as follows: in a sixty-minute SSG experiment, the solar steam generator is randomly flipped every 10 min to switch the evaporation surface. The temperature of evaporation surface (Figure 4e) and water mass loss are recorded after flipping. In order to meticulously investigate the effect of flipping on water evaporation rate, the concept of "interval mean evaporation rate" is proposed. As seen from the red dots in Figure 4f, every dot is also calculated by Formula S1, and the irradiation time (T) and initial mass of water are reset at the initial point of each interval. The results reveal that temperature of evaporation surface can quickly rise to more than 90 % of the maximum temperature within 2 min, and concurrently, the interval mean evaporation rate is recovered to near maximum. The black line in Figure 4f presents the water mass change (2.740 kg*m^{-2} h^{-1} in total) over the course of sixty-minute SSG experiment with quintuplicate flipping of the solar steam generator. It can be seen that the flipping of the solar steam generator does not have a great influence on the total water evaporation rate, meaning that the prepared solar steam generator is adequate for dealing with dynamic water environment.

In order to clarify the superiority of using hydrophile/hydrophobe amphipathic Janus nanofibers aerogels (CA//PVB-based product for short) as host materials for solar steam generators, completely hydrophilic CA nanofibers aerogel (CA-based product), hydrophobic PVB nanofibers aerogel (PVB-based product) and CA-PVB blended nanofibers aerogel (CA-PVB-based product) are also respectively fabricated and coated with photothermal materials through the same freeze drying and air spraying processes as those for preparing amphipathic Janus nanofibers aerogel. The PVB-based product cannot be used as a solar steam generator at all due to its inability to pump water. The CA-based product can pump water but cannot float on water surface. Therefore, a scaffold has to be used to immobilize the CA-based product on the water surface. CA-PVB-based product also can float on water surface by itself. The water evaporation performances of CA//PVB-based product, CA-PVB-based product and CA-based product as well as the water without using any solar steam generators (blank water), are compared. The results of water evaporation rates are shown in **Figure 5** a. The CA//PVB-based product exhibits much higher water evaporation rate than CA-PVB-based product and CA-based product (2.944 kg m^{-2} h^{-1} *vs* . 0.771 kg m^{-2} h^{-1} and 2.125 kg m^{-2} h^{-1}), and the evaporation rate of blank water is only 0.414 kg $m^{-2}h^{-1}$. Compared with CA//PVB-based product, CA-PVB-based product shows a much lower water evaporation performance, even though they have the same composition in raw materials. Through carefully observing the evaporation surface of CA-PVB-based product during SSG process, it can be found that almost no water exists on the evaporation surface, proving a poor water-pumping ability of CA-PVB-based product. As illustrated in Figure 5b, the CA components of CA//PVB Janus nanofibers facilitate rapid upward pumping of water molecules due to the closely situated hydrophilic groups on CA. As for CA-PVB blended nanofibers, the presence of PVB molecular chains results in an increased distance between hydrophilic groups, leading to a much weaker water-pumping ability. Thus, a simple blending of hydrophilic and hydrophobic materials is not applicable for fabricating solar steam generators. The relatively lower water evaporation performance of the CA-based product can be attributed to its excessive internal water content (~ 0.95 g cm^{-3}), which aggravates heat dissipation, as revealed in Figure 5c and d. In addition, it is also found that the CA-based product exhibits poor reusability, as shown in **Figure S5** . In order to explain this result, the physical photos of CA//PVB Janus nanofibers aerogel, CA nanofibers aerogel, CA//PVB-based product and CA-based product before and after water soaking are provided in **Figure S6** . After 10 cycles, the photothermal materials are seriously peeled off the CA-based product. This phenomenon is attributed to the swelling of CA nanofibers aerogel in water. After water soaking, CA-based product experiences a noticeable expansion in volume, which creates internal stress between photothermal materials and the swollen CA nanofibers aerogel and thus leads to the detachment of photothermal materials. As for the CA//PVB-based product, the hydrophobic PVB components suppresses the volume expansion of the CA components, and the entire aerogel retains almost the same morphology before and after being placed in water. Thus, photothermal materials can be stable on CA//PVB Janus nanofibers aerogel during SSG process, thereby achieving excellent reusability. From the above results, it is obvious that the hydrophile/hydrophobe amphipathic Janus nanofibers aerogels are superior for preparing solar steam generators in view of their high performance, reusability and ease of use.

2.4 Desalination and Pollutants Removal Performances

Desalination and pollutants removal performances are important application aspects of solar steam generators. Fast evaporation rate of saline water and effective inhibition on salt crystallization are crucial for desalination applications. The water evaporation performances and salt-resisting properties of CA//PVB-based product and CA-based product are comparatively studied. The 3.5 % NaCl aqueous solution, which is close to the average salinity of seawater, is adopted as a model substance. As seen from **Figure 6** a, in the first-hour SSG experiment, the water evaporation rates with CA//PVB-based product and CA-based product are 2.909 kg $m^{-2}h^{-1}$ and 1.916 kg $m^{-2}h^{-1}$, respectively. Compared with the evaporation rates of pure water when using the two kinds of solar steam generators, the evaporation rates of 3.5 % NaCl solution decrease 1.19 % and 9.84 %, respectively. From careful observation on the red curve in Figure 6a, the slope of the curve decreases with the extension of evaporation time, which means CA-based product occurs obvious performance attenuation during the process of treating saline water. In order to amplify the effect of saline water evaporation on the two solar steam generators, five-hour evaporation experiments are carried out, and the photographs of the two post-use solar steam generators are provided in Figure 6b and c. It is obviously seen that a lot of salt crystals deposit on CA-based product, whereas the situation of CA//PVB-based product is much better, demonstrating excellent salt-resisting property of CA//PVB Janus nanofibers aerogel. On the one hand, salt crystals block water transfer channels, and on the other hand, they reflect light. Both of these effects negatively impact on water evaporation. According to the references[32,46], it has been proved that hydrophobic materials can inhibit the shuttle of salt ions. Therefore, the excellent salt-resisting property of CA//PVB Janus nanofibers aerogel can be owing to the hydrophobic PVB components. To sum up, in terms of desalination property, the amphipathic Janus nanofibers aerogel also shows its superiority over the hydrophilic substrate.

The evaporation rates of saline water with different salinities when using the CA//PVB-based product are also studied. The NaCl solutions with different concentrations (1 %, 3.5 %, 5 %, 10 %, 20 %) are prepared as analytes, and the results are shown in Figure 6d. The evaporation rate decreases with the increase of salinity, but the difference is not great, which proves that the product can be able to effectively treat high-salinity water. The desalination performances of the CA//PVB-based product on saline water with different salinities are revealed in Figure 6f, and the desalination results on actual seawater (sampled from Bohai Sea, geological coordinate of sampling site: 40deg53'23.90"N, 121deg12'26.72"E) are given in Figure 6g. As revealed in**Figure S7** , the SSG process is performed in a lab-made acrylic tank (18 cm x 9 cm x 12 cm) in which the water vapor is condensed and collected at a rate of 2.227 kg $m^{-2}h^{-1}$ (this value is obtained when pure water is treated with the amphipathic Janus nanofibers aerogel under 1 sun). The results demonstrate that the concentrations of salt ions in the collected liquids greatly decrease compared with those of the original saline water and actual seawater and are much lower than the standard of the World Health Organization (WHO) and the United States Environmental Protection Agency (EPA) for salt ion concentration in drinking water. Moreover, it is also found that the prepared solar steam generator is self-cleaning in the dark. As seen from Figure 6e, after ten-hour light irradiation (close to the total energy of sunlight in a day), some visible salt crystals deposit on the surface of product, and these salt crystals disappear automatically within 4 h in the dark. This character may be owing to the large pores in the aerogel that are conducive to the rapid downward diffusion of salt ions under the driving of concentration gradient between evaporation surface and bulk water. This self-cleaning property is beneficial for performance recovery of the product with day/night changes in outdoor applications. In addition, a faster way to eliminate the influence of salt deposition is to flip the solar steam generator. That is, after the evaporation surface is altered, the water evaporation rate can be recovered quickly.

The treatment on wastewater containing antibiotics or organic dyes is another essential application of SSG. To evaluate the related performance of CA//PVB-based product, TCH, RhB and MB solutions, with the concentrations of 0.01 g L^{-1}, are selected as model substances. As reveal from Figure 6h and **Figure S8** , the removal rates of these organic contaminants are all above 99 % in the condensed water.

3. Conclusion

In summary, hydrophile/hydrophobe amphipathic Janus nanofibers aerogel is fabricated by the combination of parallel electrospinning technology and freeze drying. Photothermal materials are covered on the six surfaces of the cubic aerogel to obtain a 3D self-floating solar steam generator. The light absorption rate of the product is above 95 % in the full spectrum range. Under light irradiation, the surface temperature of the product rapidly rises to meet the requirement of fast water evaporation within 2 min. The water evaporation rate can reach up to 2.944 $kg*m^{-2}*h^{-1}$ with the energy efficiency of 91.05 % under 1 sun irradiation, and after the product is flipped, the water evaporation rate can be quickly recovered. Owing to the salt-resisting property, the formation of salt deposition can be effectively slowed down, so that the performance attenuation in the evaporation of saline water is suppressed. The product possesses excellent ability of solar desalination and removing organic pollutants to acquire drinkable water.

Conflict of Interest

The authors have no conflict of interest to declare.

Supporting Information

Supporting Information is available from the Wiley Online Library or from the author.

Acknowledgements

This work was financially supported by Natural Science Foundation of Chongqing, China (cstc2021jcyj-msxmX0898), Natural Science Foundation of Jilin Province (20210101080JC), National Natural Science Foundation of China (51803012, 51573023).

Received: ((will be filled in by the editorial staff)) Revised: ((will be filled in by the editorial staff)) Published online: ((will be filled in by the editorial staff))

References

[1] X. Wu, Y. Wang, P. Wu, J. Zhao, Y. Lu, X. Yang, H. Xu,*Adv. Funct. Mater.* **2021** , *31* , 2102618.

[2] Y. Zhang, Y. Wang, B. Yu, K. Yin, Z. Zhang, *Adv. Mater.***2022** , *34* , 2200108.

[3] N. Liu, L. Hao, B. Zhang, R. Niu, J. Gong, T. Tang, *Energy Environ. Mater.* **2022** , *5* , 617-626.

[4] M. Jin, Z. Wu, F. Guan, D. Zhang, B. Wang, N. Sheng, X. Qu, L. Deng, S. Chen, Y. Chen, H. Wang, *ACS Appl. Mater. Interfaces***2022** , *14* , 12284-12294.

[5] X. Wang, K. Liu, Z. Wang, L. Heng, L. Jiang, *J. Mater. Chem. A* **2022** , *10* , 3436-3442.

[6] H. Bai, N. Liu, L. Hao, P. He, C. Ma, R. Niu, J. Gong, T. Tang,*Energy Environ. Mater.* **2022** , *5* , 1204-1213.

[7] H. Zhang, X. Shen, E. Kim, M. Wang, J. H. Lee, H. Chen, G. Zhang, J. K. Kim, *Adv. Funct. Mater.* **2022** , *32* , 2111794.

[8] J. Yuan, X. Lei, C. Yi, H. Jiang, F. Liu, G. J. Cheng,*Chem. Eng. J.* **2022** , *430* , 132765.

[9] I. Ibrahim, S. M. Hossain, D. H. Seo, A. McDonagh, T. Foster, H. K. Shon, L. Tijing, *Sep. Purif. Technol.* **2022** ,*293* , 121054.

[10] R. Wang, J. Deng, P. Wu, Q. Ma, X. Dong, W. Yu, G. Liu, J. Wang, L. Liu, *J. Environ. Chem. Eng.* **2022** , *10* , 108173.

[11] B. Xiao, W. Zhou, F. Yu, J. Wang, X. Xiong, G. Liu, Y. Xia, X. Wang, *Environ. Prog. Sustain. Energy* **2022** , *42* , e13944.

[12] R. Zhang, B. Xiang, Y. Wang, S. Tang, X. Meng, *Mater. Horiz.* **2022** , *9* , 1232-1242.

[13] X. Zhang, L. Ren, J. Xu, B. Shang, X. Liu, W. Xu, *Small* ,**2022** , *18* , 2105198.

[14] Y. Wang, H. Ma, J. Yu, J. Li, N. Xu, J. Zhu, L. Zhou,*Adv. Opt. Mater.* **2023** , *11* , 2201907.

[15] Y. Dong, Y. Tan, K. Wang, Y. Cai, J. Li, C. Sonne, C. Li,*Water Res.* **2022** , *223* , 119011.

[16] X. Zhang, M. Pi, H. Lu, M. Li, X. Wang, Z. Wang, R. Ran,*Sol. Energy Mater. Sol. Cells* **2022** , *242* , 111742.

[17] Y. Wang, X. Wu, P. Wu, J. Zhao, X. Yang, G. Owens, H. Xu,*Sci. Bull.* **2021** , *66* , 2479-2488.

[18] X. Hu, J. Zhu, *Adv. Funct. Mater.* **2020** ,*30* , 1907234.

[19] X. Meng, W. Xu, Z. Li, J. Yang, J. Zhao, X. Zou, Y. Sun, Y. Dai, *Adv. Fiber Mater.* **2020** , *2* , 93-104.

[20] Y. Fu, G. Wang, X. Ming, X. Liu, B. Hou, T. Mei, J. Li, J. Wang, X. Wang, *Carbon* **2018** , *130* , 250-256.

[21] Z. Qin, S. Zhao, X. Fang, B. Zhao, J. Deng, K. Pan, *Adv. Funct. Mater.* **2022** , *32* , 2109240.

[22] T. Pirzada, Z. Ashrafi, W. Xie, S. A. Khan, *Adv. Funct. Mater.* **2020** , *30* , 1907359.

[23] M. Dilamian, M. Joghataei, Z. Ashrafi, C. Bohr, S. Mathur, H. Maleki, *Appl. Mater. Today* **2021** , *22* , 100964.

[24] F. Meng, H. Wang, Z. Chen, T. Li, C. Li, Y. Xuan, Z. Zhou,*Nano Res.* **2018** , *11* , 2847-2861.

[25] R. Liu, X. Dong, S. Xie, T. Jia, Y. Xue, J. Liu, W. Jing, A. Guo, *Chem. Eng. J.* **2019** , *360* , 464-472.

[26] Z. Yuan, Y. Ren, M. Shafiq, Y. Chen, H. Tang, B. Li, M. EL-Newehy, H. EL-Hamshary, Y. Morsi, H. Zheng, X. Mo, *Macromol. Biosci.* **2022** , *22* , 2100342.

[27] J. Qiu, P. Fan, C. Yue, F. Liu, A. Li, *J. Mater. Chem. A***2019** , *7* , 7053-7064.

[28] Y. Si, Q.Fu, X. Wang, J. Zhu, J. Yu, G. Sun, B. Ding, *ACS Nano* **2015** , *9* , 3791-3799.

[29] C. Li, S. Cao, J. Lutzki, J. Yang, T. Konegger, F. Kleitz, A. Thomas, *J. Am. Chem. Soc.*

2022 , *144* , 3083-3090.

[30] S. Sun, Y. Wang, B. Sun, F. Zhang, C. Shen, *ACS Appl. Mater. Interfaces* **2021** , *13* , 24945-24956.

[31] Q. Zhang, G. Yi, Z. Fu, H. Yu, X. Quan, *ACS Nano***2019** , *13* , 13196-13207.

[32] W. Xu, X. Hu, S. Zhuang, Y. Wang, X. Li, L. Zhou, S. Zhu, J. Zhu, *Adv. Energy Mater.* **2018** , *8* , 1702884.

[33] H. Jian, Q. Qi, W. Wang, D. Yu, *Sep. Purif. Technol.***2021** , *264* , 118459.

[34] B. Sun, Y. Han, S. Li, P. Xu, X. Han, A. Nafady, S. Ma, Y. Du,*J. Mater. Chem. A* **2021** , *9* , 23140-23148.

[35] B. Wen, X. Zhang, Y. Yan, Y. Huang, S. Lin, Y. Zhu, Z. Wang, B. Zhou, S. Yang, J. Liu, *Desalination* **2021** , *516* , 115228.

[36] Q. Zhou, H. Li, D. Li, B. Wang, H. Wang, J. Bai, S. Ma, G. Wang, *J. Colloid. Interf. Sci.* **2021** , *592* , 77-86.

[37] H. Yao, P. Zhang, C. Wang, Q. Liao, X. Hao, Y. Huang, M. Zhang, X. Wang, T. Lin, H. Cheng, J. Yuan, L. Qu, *Energy Environ. Sci.***2021** , *14* , 5330-5338.

[38] Q. Ma, J. Wang, X. Dong, W. Yu, G. Liu, *Adv. Funct. Mater.* **2015** , *25* , 2436-2443.

[39] P. Wu, Q. Ma, W. Yu, J. Wang, G. Liu, X. Dong, *J. Mater. Chem. C* **2021** , *9* , 7615-7621.

[40] D. G. Yu, J. J. Li, M. Zhang, G. R. Williams, *Chem. Commun.* **2017** , *53* , 4542-4545.

[41] X. Mu, Y. Gu, P. Wang, J. Shi, A. Wei, Y. Tian, J. Zhou, Y. Chen, J. Zhang, Z. Sun, *Solar RRL* **2020** , *4* , 2000341.

[42] T. Nakaoki, H. Yamashita, *J. Mol. Struct.* **2008** ,*875* , 282-287.

[43] K. Kudo, J. Ishida, G. Syuu, Y. Sekine, T. Ikeda-Fukazawa,*J. Chem. Phys.* **2014** , *140* , 158.

[44] W. B. Monosmith, G. E. Walrafen, *J. Chem. Phys.***1984** , *81* , 669-674.

[45] X. Ouyang, P. Wu, J. Deng, Q. Ma, X. Dong, W. Yu, G. Liu, J. Wang, L. Liu, *Sep. Purif. Technol.* **2022** , *297* , 121526.

[46] L. Zang, C. Finnerty, S. Zheng, K. Conway, L. Sun, J. Ma, B. Mi, *Water Res.* **2021** , *198* , 117135.

Figure Captions

Figure 1. (a) Structure diagram of the prepared solar steam generator; SEM imagery of (b) CA nanofibers, (c) PVB nanofibers, (d) CA//PVB Janus nanofibers, (e) CA//PVB Janus nanofibers aerogel, and (f-h) surface of the solar steam generator

Figure 2. (a) Densities and saturation water contents of solar steam generators; (b) water mass change curves and (c) temperature variation when using solar steam generators with different densities; (d) water mass change curves when using solar steam generators with different loading amounts of photothermal materials; (e) water evaporation performances, (f) temperature variations and (g) light absorption spectra of solar steam generators with different contents of SiO_2 NPs; (h) illustration of water state in photothermal materials; (i) mass losses of solar steam generators with different PDA contents after water soaking; (j) water evaporation performances, (k) temperature variations and (j) light absorption spectra of solar steam generators with different contents of PDA

Figure 3. (a) Water mass change curves, (b) hourly evaporation capacities and energy efficiencies, and (c) infrared thermal imaging photographs of evaporation surface and bulk water under different irradiation intensities

Figure 4. (a) Water content of the solar steam generator during SSG process; (b) hourly water evaporation rates in ten-hour continuous SSG process; (c) water evaporation rates in 20 cycles under 1 sun irradiation; (d) illustration of flipped solar steam generator in natural water environment; (e) temperature variation of evaporation surface, (f) water mass change and interval mean evaporation rate with quintuplicate flipped solar steam generator

Figure 5. (a) Water evaporation performances of contrast samples; (b) illustration of water-pumping ability of CA//PVB Janus nanofibers and CA-PVB blended nanofibers; (c) temperature variation curves and (d) infrared thermal imaging photographs of contrast samples

Figure 6. (a) Mass change curves of 3.5 % NaCl aqueous solution with or without solar steam generators; salt deposition on (b) CA-based product and (c) CA//PVB-based product after five-hour SSG; (d) evaporation rates of NaCl solutions with different concentrations when using CA//PVB-based product; (e) self-cleaning property of CA//PVB-based product; desalination performances of CA//PVB-based product on (f) NaCl solutions with different concentrations and (g) actual seawater; (h) organic compounds removal performances of CA//PVB-based product

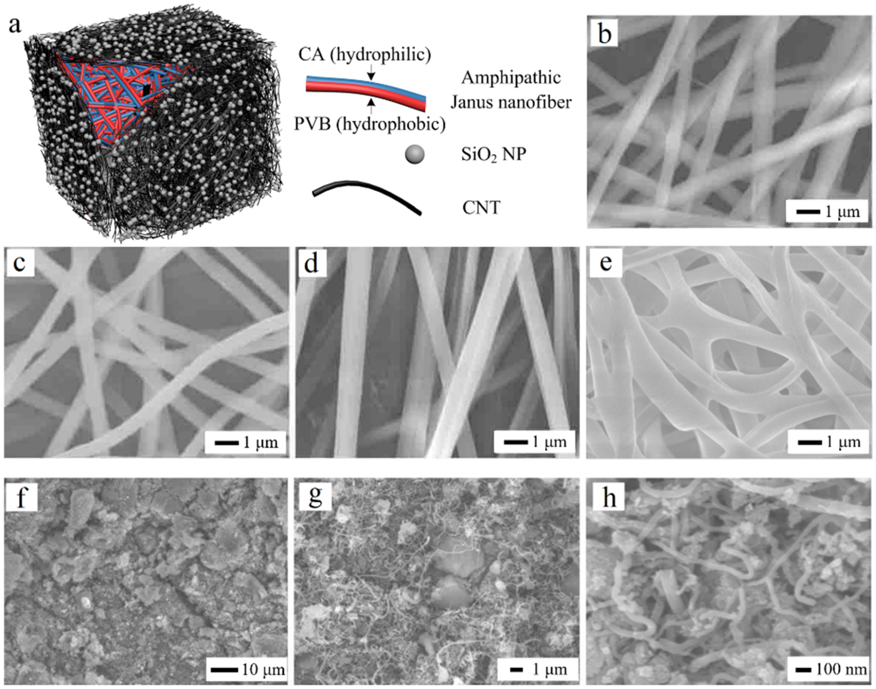
a
CA (hydrophilic)
Amphipathic
Janus nanofiber
PVB (hydrophobic)
SiO_2 NP
CNT
b
1 μm
c
1 μm
d
1 μm
e
1 μm
f
10 μm
g
1 μm
h
100 nm

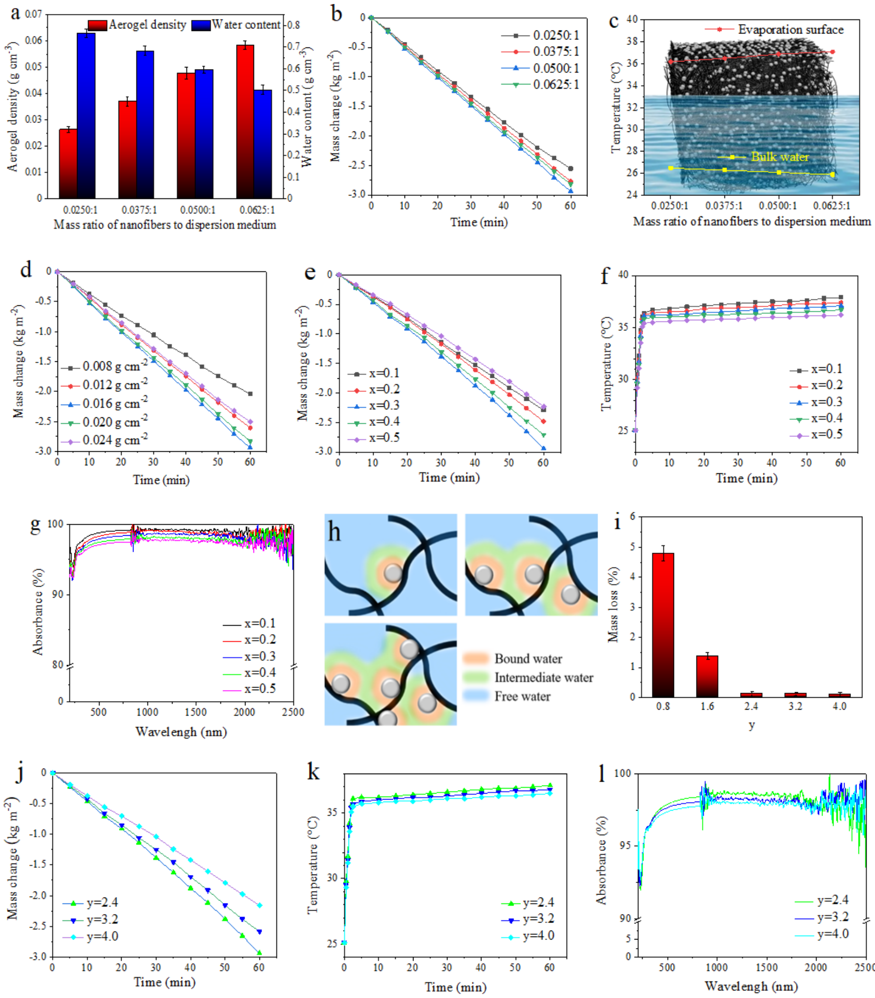
a
Aerogel density
Water content
Aerogel density (g cm^{-3})
Water content (g cm^{-3})
0.0250:1
0.0375:1
0.0500:1
0.0625:1
Mass ratio of nanofibers to dispersion medium
b
Mass change (kg m^{-2})
Time (min)
c
Evaporation surface
Bulk water
Temperature (℃)
Mass ratio of nanofibers to dispersion medium
d
0.008 g cm^{-2}
0.012 g cm^{-2}
0.016 g cm^{-2}
0.020 g cm^{-2}
0.024 g cm^{-2}
e
x=0.1
x=0.2
x=0.3
x=0.4
x=0.5
f
g
Absorbance (%)
Wavelengh (nm)
h
Bound water
Intermediate water
Free water
i
Mass loss (%)
y
j
y=2.4
y=3.2
y=4.0
k
l

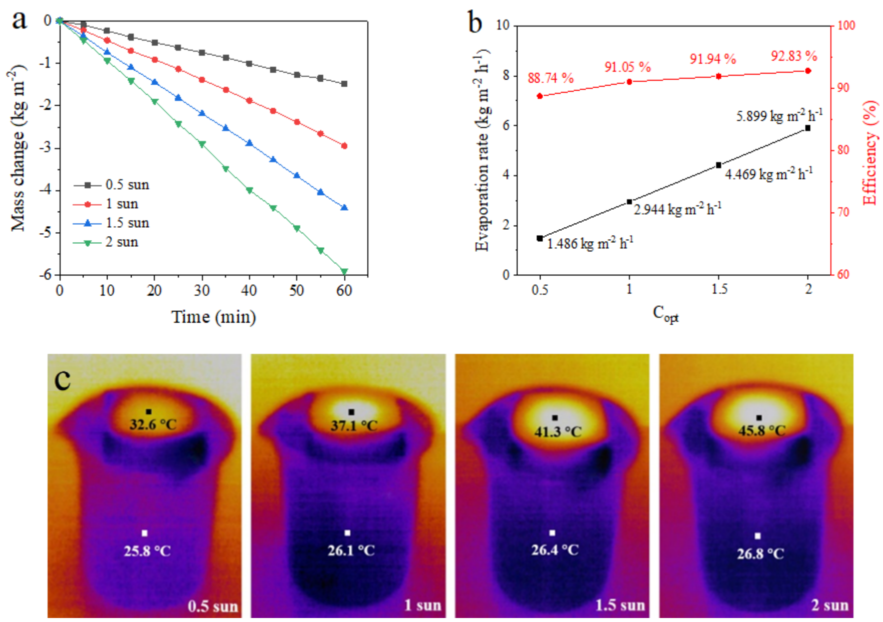
a
Mass change (kg m-2)
Time (min)
0.5 sun
1 sun
1.5 sun
2 sun
b
Evaporation rate (kg m-2 h-1)
Efficiency (%)
Copt
88.74 %
91.05 %
91.94 %
92.83 %
1.486 kg m-2 h-1
2.944 kg m-2 h-1
4.469 kg m-2 h-1
5.899 kg m-2 h-1
c
32.6 °C
25.8 °C
0.5 sun
37.1 °C
26.1 °C
1 sun
41.3 °C
26.4 °C
1.5 sun
45.8 °C
26.8 °C
2 sun

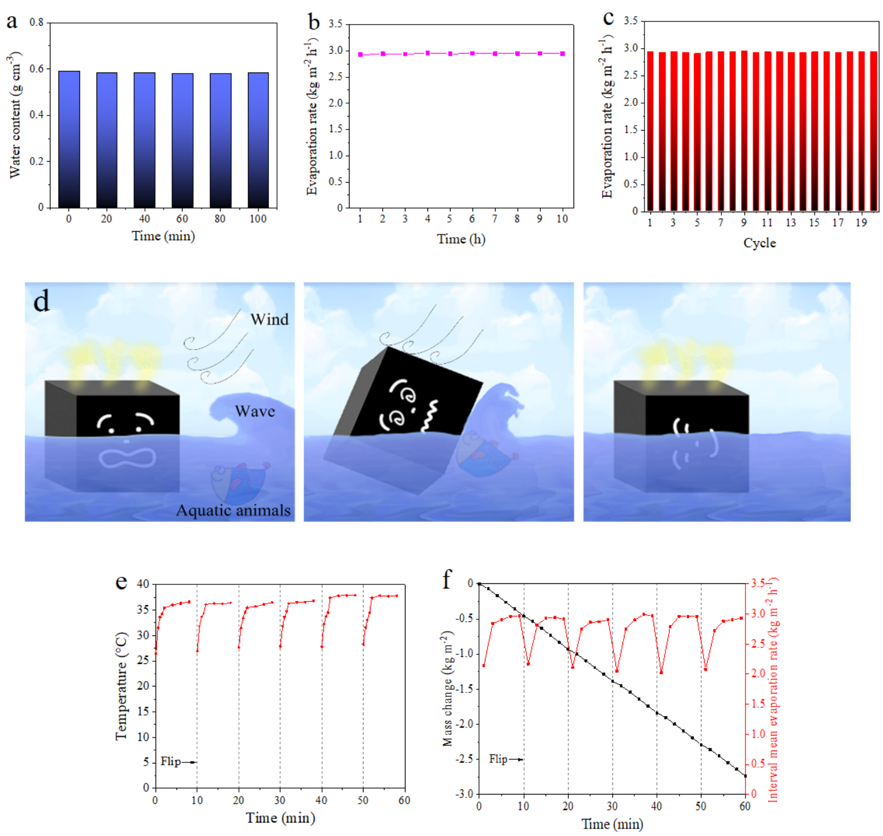
a
Water content (g cm-3)
Time (min)
b
Evaporation rate (kg m-2 h-1)
Time (h)
c
Evaporation rate (kg m-2 h-1)
Cycle
d
Wind
Wave
Aquatic animals
e
Temperature (°C)
Flip
Time (min)
f
Mass change (kg m-2)
Interval mean evaporation rate (kg m-2 h-1)
Flip
Time (min)

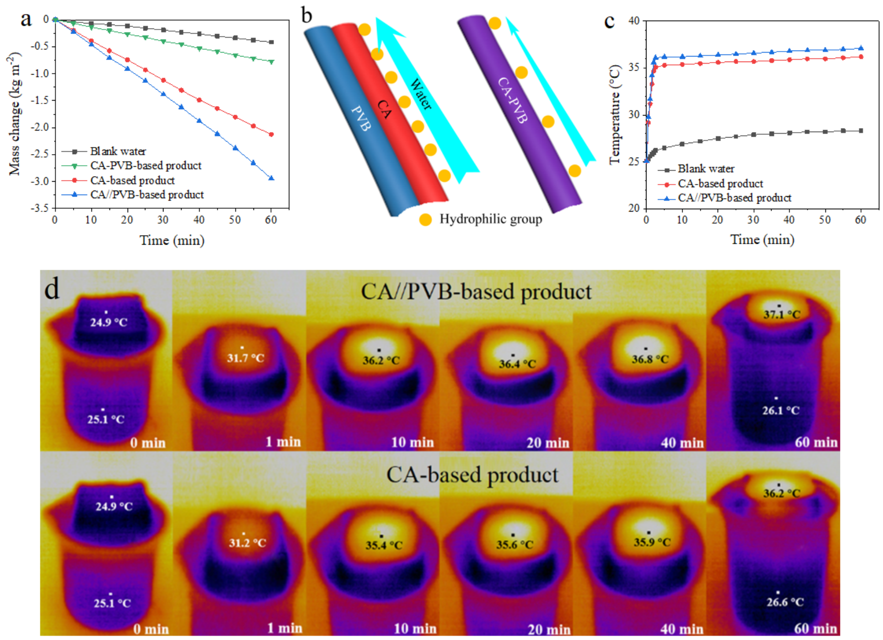
a
Mass change (kg m-2)
Time (min)
Blank water
CA-PVB-based product
CA-based product
CA//PVB-based product
b
PVB
CA
Water
CA-PVB
Hydrophilic group
c
Temperature (°C)
Time (min)
Blank water
CA-based product
CA//PVB-based product
d
CA//PVB-based product
24.9 °C
25.1 °C
0 min
31.7 °C
1 min
36.2 °C
10 min
36.4 °C
20 min
36.8 °C
40 min
37.1 °C
26.1 °C
60 min
CA-based product
24.9 °C
25.1 °C
0 min
31.2 °C
1 min
35.4 °C
10 min
35.6 °C
20 min
35.9 °C
40 min
36.2 °C
26.6 °C
60 min

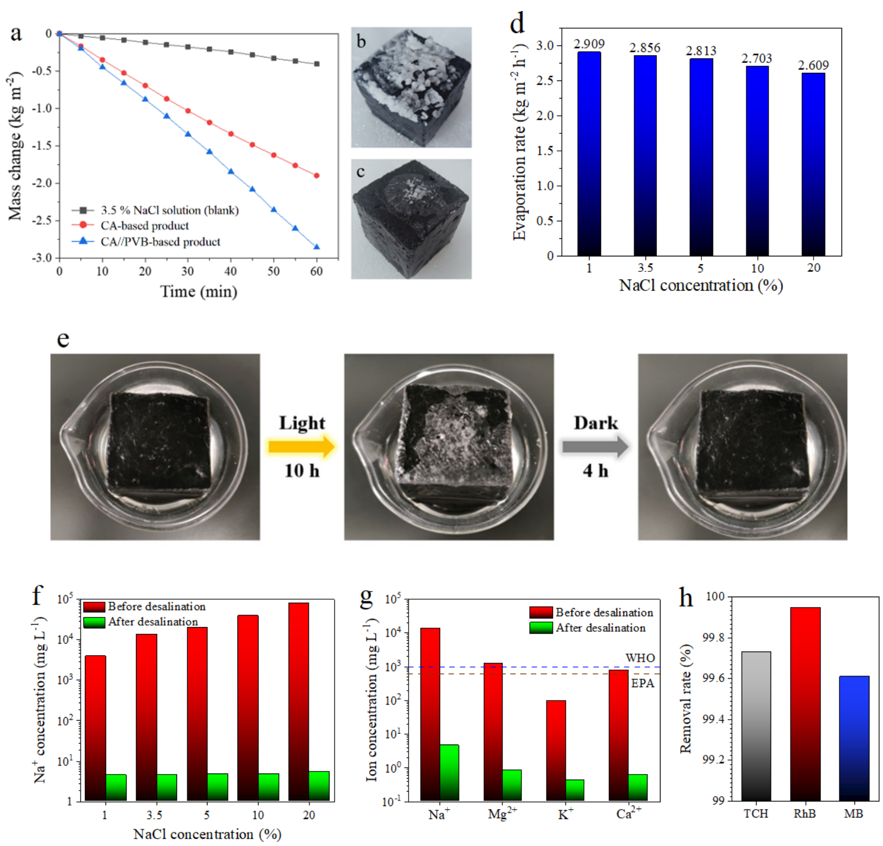
a
Mass change (kg m-2)
Time (min)
3.5 % NaCl solution (blank)
CA-based product
CA//PVB-based product
b
c
d
Evaporation rate (kg m-2 h-1)
2.909
2.856
2.813
2.703
2.609
NaCl concentration (%)
e
Light
10 h
Dark
4 h
f
Na+ concentration (mg L-1)
Before desalination
After desalination
NaCl concentration (%)
g
Ion concentration (mg L-1)
Before desalination
After desalination
WHO
EPA
Na+
Mg2+
K+
Ca2+
h
Removal rate (%)
TCH
RhB
MB